

Evolution of the $f\sigma_8$ tension with the Planck15/ Λ CDM determination and implications for modified gravity theories

Lavrentios Kazantzidis* and Leandros Perivolaropoulos†

Department of Physics, University of Ioannina, GR-45110, Ioannina, Greece

 (Received 12 March 2018; published 3 May 2018)

We construct an updated extended compilation of distinct (but possibly correlated) $f\sigma_8(z)$ redshift space distortion (RSD) data published between 2006 and 2018. It consists of 63 datapoints and is significantly larger than previously used similar data sets. After fiducial model correction we obtain the best fit $\Omega_{0m} - \sigma_8$ Λ CDM parameters and show that they are at a 5σ tension with the corresponding Planck15/ Λ CDM values. Introducing a nontrivial covariance matrix correlating randomly 20% of the RSD datapoints has no significant effect on the above tension level. We show that the tension disappears (becomes less than 1σ) when a subsample of the 20 most recently published data is used. A partial cause for this reduced tension is the fact that more recent data tend to probe higher redshifts (with higher errorbars) where there is degeneracy among different models due to matter domination. Allowing for a nontrivial evolution of the effective Newton's constant as $G_{\text{eff}}(z)/G_N = 1 + g_a(\frac{z}{1+z})^2 - g_a(\frac{z}{1+z})^4$ (g_a is a parameter) and fixing a Planck15/ Λ CDM background we find $g_a = -0.91 \pm 0.17$ from the full $f\sigma_8$ data set while the 20 earliest and 20 latest datapoints imply $g_a = -1.28^{+0.28}_{-0.26}$ and $g_a = -0.43^{+0.46}_{-0.41}$ respectively. Thus, the more recent $f\sigma_8$ data appear to favor GR in contrast to earlier data. Finally, we show that the parametrization $f\sigma_8(z) = \lambda\sigma_8\Omega(z)^\gamma/(1+z)^\beta$ provides an excellent fit to the solution of the growth equation for both GR ($g_a = 0$) and modified gravity ($g_a \neq 0$).

DOI: 10.1103/PhysRevD.97.103503

I. INTRODUCTION

A wide range of different cosmological observations [1–10] are converging to the fact that the expansion rate of the Universe is approximated to high accuracy by the Λ CDM model [11] as

$$H(z)^2 = H_0^2[\Omega_{0m}(1+z)^3 + (1 - \Omega_{0m})] \quad (1.1)$$

where H_0 is the Hubble parameter, z is the redshift and Ω_{0m} is the present matter density parameter. The best fit parameter values for Λ CDM as obtained by Planck [12] are shown in Table I and in the context of general relativity (GR) they describe the current concordance model Planck15/ Λ CDM. Despite of the consistency of the model with cosmological observations measuring the background expansion rate (eg. Type Ia Supernovae SnIa [9,13–15] and baryon acoustic oscillations [1,2]), measurements of the growth rate of cosmological density perturbations have been shown to favor parameter values that are in some tension [16–20] with the Planck15/ Λ CDM parameter values of Table I. Such probes include weak lensing [21–26] and redshift space distortion observations [16,27–31]. A simple way to account for this tension is

to allow [27] for the possibility of extensions of GR in the form of modified theories of gravity [32–44].

RSD measurements in galaxy redshift surveys [46–50] measure the peculiar velocities of matter and thus infer [51] the growth rate of cosmological perturbations on a range of redshifts and scales.

Since about 2006 most growth rate measurements are reported as the combination $f(a)\sigma_8(a)$ where a is the scale factor $a = \frac{1}{1+z}$, $f(a) \equiv d \ln \delta(a)/d \ln a$ is the growth rate of cosmological perturbations, $\delta(a) \equiv \delta\rho/\rho$ is the linear matter overdensity growth factor and σ_8 is the matter power spectrum normalization on scales of $8h^{-1}$ Mpc.

TABLE I. Planck15/ Λ CDM parameters from Ref. [12]. The corresponding WMAP7/ Λ CDM from Ref. [45] are also shown for comparison.

Parameter	Planck15/ Λ CDM [12]	WMAP7/ Λ CDM [45]
$\Omega_b h^2$	0.02225 ± 0.00016	0.02258 ± 0.00057
$\Omega_c h^2$	0.1198 ± 0.0015	0.1109 ± 0.0056
n_s	0.9645 ± 0.0049	0.963 ± 0.014
H_0	67.27 ± 0.66	71.0 ± 2.5
Ω_{0m}	0.3156 ± 0.0091	0.266 ± 0.025
w	–1	–1
σ_8	0.831 ± 0.013	0.801 ± 0.030

*lkazantzi@cc.uoi.gr

†leandros@uoi.gr

RSDs lead to anisotropies of the power spectrum of perturbations which may lead to the values of $f\sigma_8$ by expanding to Legendre polynomials up to order four and assuming that the true underlying matter power spectrum is isotropic while the anisotropy is due only to the peculiar velocities of galaxies that distort the galaxy distribution in redshift space.

In practice however the anisotropy of the power spectrum on large scales is not only due to the peculiar galactic velocities but also due to the use of an incorrect fiducial cosmology $H(z)$ assumed in converting the measured angles and redshifts into comoving coordinates in order to construct the correlation function and the corresponding power spectrum [28,52,53]. In particular, the comoving distance between a pair of galaxies separated by an angle $d\theta$ is obtained from the Friedmann Robertson Walker (FRW) metric as [54–56]

$$d\ell_{\perp} = (1+z)D_A(z)d\theta \quad (1.2)$$

where $D_A(z)$ is the angular diameter distance at the redshift of the pair. Also the corresponding separation along the line of sight is

$$d\ell_{\parallel} = \frac{cdz}{H(z)} \quad (1.3)$$

where $H(z)$ is the true Hubble expansion rate of the true underlying cosmology. If a different (fiducial) cosmology $H'(z)$ is assumed instead, the corresponding separations become

$$d\ell'_{\perp} = (1+z)D'_A d\theta = \left(\frac{D'_A}{D_A}\right) d\ell_{\perp} = \frac{d\ell'_{\perp}}{f_{\perp}}, \quad (1.4)$$

$$d\ell'_{\parallel} = \frac{cdz}{H'} = \left(\frac{H}{H'}\right) d\ell_{\parallel} = \frac{d\ell'_{\parallel}}{f_{\parallel}} \quad (1.5)$$

where $F \equiv f_{\parallel}/f_{\perp}$ is the induced anisotropy due to the use of incorrect fiducial cosmology and has magnitude [52]

$$F = \frac{f_{\parallel}}{f_{\perp}} = \left(\frac{H'}{H}\right) \left(\frac{D'_A}{D_A}\right) \quad (1.6)$$

This induced anisotropy due to the use of incorrect fiducial cosmology is the Alcock-Paczynski (AP) effect [57] and is degenerate with the RSD anisotropy induced by the galactic peculiar velocities due to the growth of structures [56]. Thus if an $f\sigma'_8$ measurement has been obtained assuming a fiducial Λ CDM cosmology $H'(z)$, the corresponding $f\sigma_8$ obtained with the true cosmology $H(z)$ is approximated as [28]

$$f\sigma_8(z) \simeq \frac{H(z)D_A(z)}{H'(z)D'_A(z)} f\sigma'_8(z) \equiv q(z, \Omega_{0m}, \Omega'_{0m}) f\sigma'_8(z) \quad (1.7)$$

This equation should be taken as a rough order of magnitude estimate of the AP effect as it appears in somewhat different forms in the literature [54–56]. In Appendix we discuss alternative forms of the correction factor [55,56].

As discussed in Sec. III, this correction is small (at most it can be about 2–3% at redshifts $z \simeq 1$ for reasonable values of Ω_{0m}). However we include it in the present analysis and we estimate its effect on the best fit cosmological parameter values.

A compilation of 63 $f\sigma_8$ measurements published by various surveys from 2006 to present is shown in Table II along with the corresponding fiducial cosmology assumed in each case. Despite of the existence of such a large sample of published $f\sigma_8$ data, most previous analyses [27,31,34,56,58–68] that use growth data to constrain cosmological models use less than 20 data points which are usually selected from the larger data set of Table II on the basis of subjective criteria that favor more recent data as well as a qualitative minimization of correlations among the selected data points. Indeed, since many of these data points are correlated due to overlap in the galaxy samples used for their derivation, a large covariance matrix should be used for their combined analysis. However no full covariance matrix is available in the literature for the data set of Table II and for almost all of its subsets. In addition the use of different fiducial models by different surveys at different times is also a source of uncertainty when using large $f\sigma_8$ samples.

Despite these problems, the use of *ad hoc* subsamples of the full $f\sigma_8$ data set of Table II may lead to a waste of useful information. Therefore, it would be interesting to perform a more detailed analysis of the full $f\sigma_8$ sample to identify possible trends of best fit parameters in the context of different subsamples, as well as to study the effects of fiducial cosmology or correlation among data points.

In particular the following open questions are of interest:

- (1) What is a complete data set of the published $f\sigma_8$ data?
- (2) What is the tension level of the best fit Λ CDM $\Omega_{0m} - \sigma_8$ obtained from the full growth data set with Planck15/ Λ CDM?
- (3) What is the effect of a typical covariance matrix on the level of the above tension?
- (4) Is the tension level the same for early and more recently published RSD $f\sigma_8$ data? Is the consistency with GR improving with time of publication of data points?
- (5) How is the tension level affected by the $f\sigma_8$ correction imposed for the different fiducial cosmologies used in each survey?
- (6) Is the spread of the $f\sigma_8$ data consistent with the published error bars?

A large part of the present analysis is devoted to the study of these questions. In addition we search for a proper parametrization of $f\sigma_8(z)$ that can represent the predictions

TABLE II. A compilation of RSD data that we found published from 2006 since 2018.

Index	Dataset	z	$f\sigma_8(z)$	References	Year	Fiducial Cosmology
1	SDSS-LRG	0.35	0.440 ± 0.050	[69]	30 October 2006	$(\Omega_{0m}, \Omega_K, \sigma_8) = (0.25, 0, 0.756)$ [70]
2	VVDS	0.77	0.490 ± 0.18	[69]	6 October 2009	$(\Omega_{0m}, \Omega_K, \sigma_8) = (0.25, 0, 0.78)$
3	2dFGRS	0.17	0.510 ± 0.060	[69]	6 October 2009	$(\Omega_{0m}, \Omega_K) = (0.3, 0, 0.9)$
4	2MRS	0.02	0.314 ± 0.048	[71,72]	13 November 2010	$(\Omega_{0m}, \Omega_K, \sigma_8) = (0.266, 0, 0.65)$
5	SnIa + IRAS	0.02	0.398 ± 0.065	[72,73]	20 October 2011	$(\Omega_{0m}, \Omega_K, \sigma_8) = (0.3, 0, 0.814)$
6	SDSS-LRG-200	0.25	0.3512 ± 0.0583	[74]	9 December 2011	$(\Omega_{0m}, \Omega_K, \sigma_8) = (0.276, 0, 0.8)$
7	SDSS-LRG-200	0.37	0.4602 ± 0.0378	[74]	9 December 2011	
8	SDSS-LRG-60	0.25	0.3665 ± 0.0601	[74]	9 December 2011	$(\Omega_{0m}, \Omega_K, \sigma_8) = (0.276, 0, 0.8)$
9	SDSS-LRG-60	0.37	0.4031 ± 0.0586	[74]	9 December 2011	
10	WiggleZ	0.44	0.413 ± 0.080	[45]	12 June 2012	$(\Omega_{0m}, h, \sigma_8) = (0.27, 0.71, 0.8)$
11	WiggleZ	0.60	0.390 ± 0.063	[45]	12 June 2012	$C_{ij} = \text{Eq. (3.3)}$
12	WiggleZ	0.73	0.437 ± 0.072	[45]	12 June 2012	
13	6dFGS	0.067	0.423 ± 0.055	[75]	4 July 2012	$(\Omega_{0m}, \Omega_K, \sigma_8) = (0.27, 0, 0.76)$
14	SDSS-BOSS	0.30	0.407 ± 0.055	[76]	11 August 2012	$(\Omega_{0m}, \Omega_K, \sigma_8) = (0.25, 0, 0.804)$
15	SDSS-BOSS	0.40	0.419 ± 0.041	[76]	11 August 2012	
16	SDSS-BOSS	0.50	0.427 ± 0.043	[76]	11 August 2012	
17	SDSS-BOSS	0.60	0.433 ± 0.067	[76]	11 August 2012	
18	Vipers	0.80	0.470 ± 0.080	[77]	9 July 2013	$(\Omega_{0m}, \Omega_K, \sigma_8) = (0.25, 0, 0.82)$
19	SDSS-DR7-LRG	0.35	0.429 ± 0.089	[78]	8 August 2013	$(\Omega_{0m}, \Omega_K, \sigma_8) = (0.25, 0, 0.809)$ [79]
20	GAMA	0.18	0.360 ± 0.090	[80]	22 September 2013	$(\Omega_{0m}, \Omega_K, \sigma_8) = (0.27, 0, 0.8)$
21	GAMA	0.38	0.440 ± 0.060	[80]	22 September 2013	
22	BOSS-LOWZ	0.32	0.384 ± 0.095	[81]	17 December 2013	$(\Omega_{0m}, \Omega_K, \sigma_8) = (0.274, 0, 0.8)$
23	SDSS DR10 and DR11	0.32	0.48 ± 0.10	[81]	17 December 2013	$(\Omega_{0m}, \Omega_K, \sigma_8) = (0.274, 0, 0.8)$ [82]
24	SDSS DR10 and DR11	0.57	0.417 ± 0.045	[81]	17 December 2013	
25	SDSS-MGS	0.15	0.490 ± 0.145	[83]	30 January 2015	$(\Omega_{0m}, h, \sigma_8) = (0.31, 0.67, 0.83)$
26	SDSS-veloc	0.10	0.370 ± 0.130	[84]	16 June 2015	$(\Omega_{0m}, \Omega_K, \sigma_8) = (0.3, 0, 0.89)$ [85]
27	FastSound	1.40	0.482 ± 0.116	[86]	25 November 2015	$(\Omega_{0m}, \Omega_K, \sigma_8) = (0.27, 0, 0.82)$ [87]
28	SDSS-CMASS	0.59	0.488 ± 0.060	[88]	8 July 2016	$(\Omega_{0m}, h, \sigma_8) = (0.307115, 0.6777, 0.8288)$
29	BOSS DR12	0.38	0.497 ± 0.045	[2]	11 July 2016	$(\Omega_{0m}, \Omega_K, \sigma_8) = (0.31, 0, 0.8)$
30	BOSS DR12	0.51	0.458 ± 0.038	[2]	11 July 2016	
31	BOSS DR12	0.61	0.436 ± 0.034	[2]	11 July 2016	
32	BOSS DR12	0.38	0.477 ± 0.051	[89]	11 July 2016	$(\Omega_{0m}, h, \sigma_8) = (0.31, 0.676, 0.8)$
33	BOSS DR12	0.51	0.453 ± 0.050	[89]	11 July 2016	
34	BOSS DR12	0.61	0.410 ± 0.044	[89]	11 July 2016	
35	Vipers v7	0.76	0.440 ± 0.040	[55]	26 October 2016	$(\Omega_{0m}, \sigma_8) = (0.308, 0.8149)$
36	Vipers v7	1.05	0.280 ± 0.080	[55]	26 October 2016	
37	BOSS LOWZ	0.32	0.427 ± 0.056	[90]	26 October 2016	$(\Omega_{0m}, \Omega_K, \sigma_8) = (0.31, 0, 0.8475)$
38	BOSS CMASS	0.57	0.426 ± 0.029	[90]	26 October 2016	
39	Vipers	0.727	0.296 ± 0.0765	[91]	21 November 2016	$(\Omega_{0m}, \Omega_K, \sigma_8) = (0.31, 0, 0.7)$
40	6dFGS + SnIa	0.02	0.428 ± 0.0465	[92]	29 November 2016	$(\Omega_{0m}, h, \sigma_8) = (0.3, 0.683, 0.8)$
41	Vipers	0.6	0.48 ± 0.12	[93]	16 December 2016	$(\Omega_{0m}, \Omega_b, n_s, \sigma_8) = (0.3, 0.045, 0.96, 0.831)$ [12]
42	Vipers	0.86	0.48 ± 0.10	[93]	16 December 2016	
43	Vipers PDR-2	0.60	0.550 ± 0.120	[94]	16 December 2016	$(\Omega_{0m}, \Omega_b, \sigma_8) = (0.3, 0.045, 0.823)$
44	Vipers PDR-2	0.86	0.400 ± 0.110	[94]	16 December 2016	
45	SDSS DR13	0.1	0.48 ± 0.16	[95]	22 December 2016	$(\Omega_{0m}, \sigma_8) = (0.25, 0.89)$ [85]
46	2MTF	0.001	0.505 ± 0.085	[96]	16 June 2017	$(\Omega_{0m}, \sigma_8) = (0.3121, 0.815)$
47	Vipers PDR-2	0.85	0.45 ± 0.11	[97]	31 July 2017	$(\Omega_b, \Omega_{0m}, h) = (0.045, 0.30, 0.8)$
48	BOSS DR12	0.31	0.469 ± 0.098	[48]	15 September 2017	$(\Omega_{0m}, h, \sigma_8) = (0.307, 0.6777, 0.8288)$
49	BOSS DR12	0.36	0.474 ± 0.097	[48]	15 September 2017	
50	BOSS DR12	0.40	0.473 ± 0.086	[48]	15 September 2017	
51	BOSS DR12	0.44	0.481 ± 0.076	[48]	15 September 2017	
52	BOSS DR12	0.48	0.482 ± 0.067	[48]	15 September 2017	
53	BOSS DR12	0.52	0.488 ± 0.065	[48]	15 September 2017	
54	BOSS DR12	0.56	0.482 ± 0.067	[48]	15 September 2017	
55	BOSS DR12	0.59	0.481 ± 0.066	[48]	15 September 2017	

(Table continued)

TABLE II. (*Continued*)

Index	Dataset	z	$f\sigma_8(z)$	References	Year	Fiducial Cosmology
56	BOSS DR12	0.64	0.486 ± 0.070	[48]	15 September 2017	
57	SDSS DR7	0.1	0.376 ± 0.038	[98]	12 December 2017	$(\Omega_{0m}, \Omega_b, \sigma_8) = (0.282, 0.046, 0.817)$
58	SDSS-IV	1.52	0.420 ± 0.076	[99]	8 January 2018	$(\Omega_{0m}, \Omega_b h^2, \sigma_8) = (0.26479, 0.02258, 0.8)$
59	SDSS-IV	1.52	0.396 ± 0.079	[100]	8 January 2018	$(\Omega_{0m}, \Omega_b h^2, \sigma_8) = (0.31, 0.022, 0.8225)$
60	SDSS-IV	0.978	0.379 ± 0.176	[101]	9 January 2018	$(\Omega_{0m}, \sigma_8) = (0.31, 0.8)$
61	SDSS-IV	1.23	0.385 ± 0.099	[101]	9 January 2018	
62	SDSS-IV	1.526	0.342 ± 0.070	[101]	9 January 2018	
63	SDSS-IV	1.944	0.364 ± 0.106	[101]	9 January 2018	

of a wide range of cosmological models including models of modified gravity.

It is well known [102–107] that the growth rate $f(z)$ of cosmological perturbations in the context of general relativity is well approximated by a parametrization of the following form

$$f(a) = \Omega_m(a)^{\gamma(a)} \quad (1.8)$$

$$\Omega_m(a) \equiv \frac{\Omega_{0m} a^{-3}}{H(a)^2/H_0^2} \quad (1.9)$$

$$\gamma(a) = \frac{\ln f(a)}{\ln \Omega_m(a)} \simeq 0.55 \quad (1.10)$$

where we have assumed Λ CDM background cosmology.

The construction of a corresponding parametrization that approximates well the theoretically predicted form of $f\sigma_8(z)$ for a wide range of theoretical models is an interesting open question that is addressed in the present analysis.

The structure of this paper is the following: In the next section we review the equations that determine the growth of matter perturbations in GR and in modified gravity theories as parametrized by the effective Newton's constant G_{eff} . We compare the numerical solution for $f\sigma_8(z)$ in the context of different cosmological models and present a new parametrization for $f\sigma_8(z)$ which provides an excellent fit to the numerical solution of $f\sigma_8$ for both Λ CDM and modified gravity models. This parametrization may be viewed as an extension for the corresponding parametrization Eq. (1.8) for the growth rate $f(a)$. In Sec. III we present a detailed analysis of the data set of Table II addressing the questions stated above using appropriate statistics. Finally in Sec. IV we summarize and discuss implications and future prospects of our results.

II. THEORETICAL PREDICTIONS OF $f\sigma_8(z)$

The Planck15/ Λ CDM concordance background model described by Eq. (1.1) with parameters from Table I can be reproduced by a wide range of theoretical models including models with dynamical and/or clustering dark energy and modified gravity models. In order to efficiently discriminate

among these classes of models, the evolution of matter density perturbations must be considered and its theoretically predicted evolution must be compared with cosmological observations. The equation that describes the evolution of the linear matter growth factor $\delta \equiv \delta\rho/\rho$ in the context of both GR and most modified gravity theories is of the form

$$\ddot{\delta} + 2H\dot{\delta} - 4\pi G_{\text{eff}}\rho\delta \approx 0 \quad (2.1)$$

where ρ is the background matter density and G_{eff} is the effective Newton's constant which in general may depend on both redshift z and cosmological scale k . Equation (2.1) in terms of the redshift z takes the following form

$$\delta'' + \left(\frac{(H^2)'}{2H^2} - \frac{1}{1+z} \right) \delta' \approx \frac{3}{2} (1+z) \frac{H_0^2 G_{\text{eff}}(z, k)}{H^2 G_N} \Omega_{0m} \delta \quad (2.2)$$

The effective Newton's constant arises from a generalized Poisson equation of the following form

$$\nabla^2 \phi \approx 4\pi G_{\text{eff}} \rho \delta, \quad (2.3)$$

where ϕ is the perturbed metric potential in the Newtonian gauge defined via the perturbed FRW metric

$$ds^2 = -(1 + 2\phi)dt^2 + a^2(1 - 2\psi)d\vec{x}^2 \quad (2.4)$$

In GR we have a constant homogeneous $G_{\text{eff}}(z, k) = G_N$ (G_N is Newton's constant as measured by local experiments) while in modified gravity theories G_{eff}/G_N may vary in both cosmological times (redshifts) and scales. In terms of the scale factor instead of redshift, Eq. (2.2) may be expressed as

$$\delta''(a) + \left(\frac{3}{a} + \frac{H'(a)}{H(a)} \right) \delta'(a) - \frac{3\Omega_{0m} G_{\text{eff}}(a, k)/G_N}{2a^5 H(a)^2/H_0^2} \delta(a) = 0 \quad (2.5)$$

For example in a modified gravity theory with action of the form

$$S = \int d^4x \sqrt{-g} \left(\frac{1}{2} f(R, \phi, X) + \mathcal{L}_m \right), \quad (2.6)$$

where $X = -g^{\mu\nu} \partial_\mu \phi \partial_\nu \phi$, G_{eff} is expressed as

$$G_{\text{eff}}(a, k)/G_N = \frac{1}{F} \frac{f_{,X} + 4(f_{,X} \frac{k^2 F_{,R}}{a^2 F} + \frac{F_{,\phi}^2}{F})}{f_{,X} + 3(f_{,X} \frac{k^2 F_{,R}}{a^2 F} + \frac{F_{,\phi}^2}{F})}, \quad (2.7)$$

where $F = F(R, \phi, X) = \partial_R f(R, \phi, X)$ and $F_{,\phi} = \partial_\phi F(R, \phi, X)$. For scalar-tensor theories [38,108–111] with Lagrangian density

$$\mathcal{L}^{\text{ScT}} = \frac{F(\phi)}{2} R + X - U(\phi) \quad (2.8)$$

G_{eff}/G_N takes the form

$$G_{\text{eff}}(a, k)/G_N = \frac{1}{F(\phi)} \frac{F(\phi) + 2F_{,\phi}^2}{F(\phi) + \frac{3}{2}F_{,\phi}^2}. \quad (2.9)$$

Solar system tests impose the following constraint on G_{eff} [112]

$$\left| \frac{1}{G_N} \frac{dG_{\text{eff}}(z)}{dz} \right|_{z=0} < 10^{-3} h^{-1} \quad (2.10)$$

while the second derivative is effectively unconstrained since [112]

$$\left| \frac{1}{G_N} \frac{d^2 G_{\text{eff}}(z)}{dz^2} \right|_{z=0} < 10^5 h^{-2} \quad (2.11)$$

In addition, nucleosynthesis constraints [113] imply that at 1σ

$$|G_{\text{eff}}/G_N - 1| \leq 0.2 \quad (2.12)$$

These constraints are respected by a parametrization of $G_{\text{eff}}(z)$ of the form [27]

$$\begin{aligned} \frac{G_{\text{eff}}(a, g_a, n)}{G_N} &= 1 + g_a(1-a)^n - g_a(1-a)^{n+m} \\ &= 1 + g_a \left(\frac{z}{1+z} \right)^n - g_a \left(\frac{z}{1+z} \right)^{n+m}. \end{aligned} \quad (2.13)$$

where n, m are integer parameters with $n \geq 2$ and $m > 0$. In what follows we set $n = m = 2$. For these parameter values, the parameter g_a is constrained by the integrated Sachs-Wolfe effect from the CMB power spectrum to be $g_a < 0.5$ [27].

The observable quantity $f\sigma_8(a)$ can be derived from the solution $\delta(a)$ of Eq. (2.5) using the definitions $f(a) \equiv d \ln \delta(a)/d \ln a$ and $\sigma(a) = \sigma_8 \frac{\delta(a)}{\delta(1)}$. Hence [114]

$$f\sigma_8(a) \equiv f(a) \cdot \sigma(a) = \frac{\sigma_8}{\delta(1)} a \delta'(a), \quad (2.14)$$

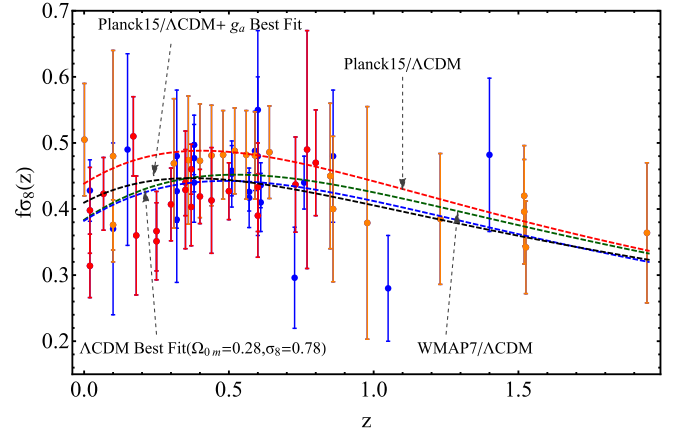


FIG. 1. Plot of $f\sigma_8(z)$ for the full growth rate data set. The green dashed line and the red dashed one correspond to the best fits of WMAP7/ Λ CDM and Planck15/ Λ CDM models respectively whereas the blue one describes the best fit Λ CDM ($\Omega_{0m} = 0.28 \pm 0.02$) to the full growth data set and the black one to the Planck15/ Λ CDM with g_a best fit. The red points correspond to the 20 earliest published points whereas the orange ones to the 20 latest published points taking into account Table II.

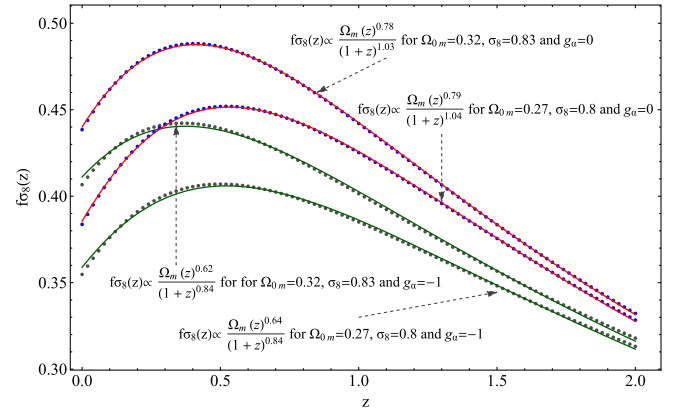


FIG. 2. Parametrization (2.15) for Planck15/ Λ CDM and WMAP7/ Λ CDM. The thick blue dots of the upper (lower) curve correspond to the numerical solution of $f\sigma_8(z)$ for Planck15/ Λ CDM (WMAP7/ Λ CDM) superposed with the analytic form (2.15) (red lines) assuming GR, whereas the gray ones of the upper (lower) curve represent the numerical solution of $f\sigma_8(z)$ for Planck15/ Λ CDM (WMAP7/ Λ CDM) superposed with the analytic form (2.15) (green lines) for modified gravity, i.e., $g_a = -1$.

Therefore the prediction of $f\sigma_8(a)$ [or equivalently $f\sigma_8(z)$] is obtained by solving numerically Eq. (2.14)¹ in the range $a \in [0, 1]$ with initial conditions assuming GR and matter domination (we set initially $\delta(a) \simeq a$)

¹There are analytic solutions of Eq. (2.14) expressed in terms of hypergeometric functions for specific cosmological models including Λ CDM [107,114–116].

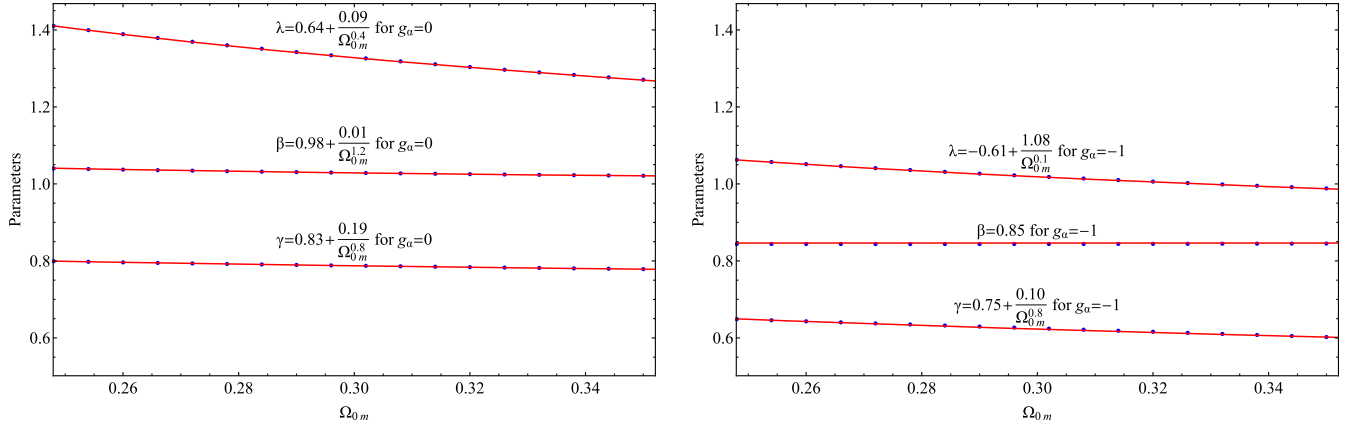


FIG. 3. The dependence of the parameters λ (upper curve), β (middle curve) and γ (lower curve) on Ω_{0m} . The blue dots are the numerically obtained values while the continuous (red) lines correspond to the best fit power laws for GR (left figure) and modified gravity (right figure), i.e., $g_a = -1$. In the two plots we use the same range for comparison.

and using Eq. (2.14). The $f\sigma_8(z)$ solutions for a Planck15/ Λ CDM and for WMAP7/ Λ CDM background cosmology $H(z)$ are shown in Fig. 1 along with the data of Table II.

Notice that WMAP7/ Λ CDM appears to be more consistent with the full $f\sigma_8$ data set than Planck15/ Λ CDM which appears to predict a larger $f\sigma_8$ than favored by the data. This well known tension will be analysed in detail in the next section.

Even though there are analytic solutions to Eq. (2.5) expressed in terms of hypergeometric functions [107,114–116] it would be useful to provide a parametrization for $f\sigma_8(z)$ in analogy with the $f(z)$ parametrization of Eq. (1.8). In view of the fact that $\sigma_8(a) \sim \delta(a)$ while $\delta(a) \sim a = \frac{1}{1+z}$ in a flat matter dominated universe, it is natural to anticipate a parametrization of the form

$$f\sigma_8(z) = \lambda\sigma_8 \frac{\Omega_m(z)^\gamma}{(1+z)^\beta} \quad (2.15)$$

where

$$\Omega_m(z) = \frac{\Omega_{0m}(z+1)^3}{\Omega_{0m}(z+1)^3 + 1 - \Omega_{0m}} \quad (2.16)$$

and λ , β , γ are parameters to be determined for given cosmological model. The parametrization (2.15) provides an excellent fit to the numerical solution $f\sigma_8(z)$. This is demonstrated in Fig. 2 where we show the numerical solution for $f\sigma_8(z)$ (dotted lines) for Planck15/ Λ CDM and WMAP7/ Λ CDM (GR is assumed $g_a = 0$) superposed with the analytic form (2.16) (continuous red lines) for $\gamma \simeq 0.78$ and $\beta \simeq 1$ (the exact parameter values are shown on the figure caption for each case).

Similarly, under the assumption of modified gravity ($g_a = -1$),² the numerical solution (dotted lines) is shown

²This value for g_a is motivated from the analysis of Ref. [27] that indicated that such a value of g_a can reduce the tension between the $f\sigma_8$ data and a Planck15/ Λ CDM $H(z)$ background.

in the same figure for the same backgrounds $H(z)$ superposed with the corresponding analytic parametrization (continuous green lines).

The parametrization (2.15) continues to provide still an excellent fit but for somewhat lower values of the parameters ($\beta \simeq 0.84$, $\gamma \simeq 0.63$). Next, in Fig. 3, we show the dependence of the parameters λ , β , γ on Ω_{0m} for $g_a = 0$ and $g_a = -1$. The dots are numerically obtained values and the continuous lines are power laws that describe the dependence of the parameters on Ω_{0m} . In the range $\Omega_{0m} \in [0.25, 0.35]$ and assuming GR ($g_a = 0$) we have $\gamma = 0.78 \pm 0.01$, $\lambda = 1.3 \pm 0.1$, $\beta = 1.03 \pm 0.01$.

III. CONSISTENCY OF RSD DATA WITH PLANCK15/ Λ CDM: TRENDS AND STATISTICS

A. Trends and inhomogeneities in the $f\sigma_8$ data

The full RSD $f\sigma_8$ dataset of Table II could be used directly to identify the best fit form of the background cosmology $H(z)$ and/or the best fit form of $G_{\text{eff}}(z)$ using the numerical solution of Eq. (2.5) to construct the predicted $f\sigma_8(z)$ with Eq. (2.14) and fitting it to the data of Table II. The results of such a brute force approach should be interpreted with care as they are affected by three factors that may lead to misleading results

- (1) Correlations among data points: As mentioned in the Introduction, the covariance matrix for the data points of Table II is not known. This is a source of uncertainty when fitting cosmological models to either the full set of data or to subsets of it.
- (2) Fiducial model correction: The different fiducial cosmologies for $f\sigma_8$ data points shown in Table II introduce another source of uncertainty that needs to be taken into account when estimating the tension with Planck15/ Λ CDM. A proper account of this effect would require a full reconstruction of the

correlation function under a Planck15/ Λ CDM fiducial cosmology for all data points of Table II. Alternatively, an approximate correction would be to include an AP correction factor, i.e., Eq. (1.7).

- (3) Survey systematics: Systematics of surveys that may vary with time of publication and may lead to data inhomogeneities.

In this section we estimate the magnitude of these effects on the tension level of the full $f\sigma_8$ data set with Planck15/ Λ CDM and on the best fit values of the parameters $\Omega_{0m} - \sigma_8$.

We use the full $f\sigma_8$ data set of Table II to obtain the best fit $\Omega_{0m} - \sigma_8$ parameters in the context of a Λ CDM background using the maximum likelihood method. Our method involves the following steps:

- (i) Solve Eq. (2.5) numerically and using Eq. (2.14) obtain $f\sigma_8(z, \Omega_{0m}, \sigma_8, g_a)$ assuming a Λ CDM background. In this subsection we consider GR and set $g_a = 0$ but in the next subsection we consider also a G_{eff} that is allowed to have a redshift dependence in accordance with the parametrization (2.13).
- (ii) Multiply the $f\sigma_8$ data of Table II (and their error bars) by the fiducial correction factor $q(z, \Omega_{0m}, \Omega_{0m}^{\text{fid}}) = \frac{H(z)D_A(z)}{H^{\text{fid}}(z)D_A^{\text{fid}}(z)}$ in accordance with Eq. (1.7) where the denominator is obtained from the fiducial Λ CDM model of each survey and the numerator involves the Ω_{0m} parameter to be fit. In practice this factor differs from unity by not more than 2%–3% and thus as it will be seen below it does not affect the tension between Planck15/ Λ CDM and the growth best fit Λ CDM model.
- (iii) As a first step for the construction of χ^2 to be minimized, construct the vector

$$V^i(z_i, \Omega_{0m}, \sigma_8, g_a) \equiv f\sigma_{8i} - \frac{f\sigma_8(z_i, \Omega_{0m}, \sigma_8, g_a)}{q(z, \Omega_{0m}, \Omega_{0m}^{\text{fid}})} \quad (3.1)$$

where we have divided the theoretical prediction $f\sigma_8(z_i, \Omega_{0m}, \sigma_8, g_a)$ by the correction factor q instead of the equivalent multiplication of the data point $f\sigma_{8i}$ (and its error bar) by the same correction factor q .

- (iv) Construct the χ^2 to be minimized as

$$\chi^2 = V^i C_{ij}^{-1} V^j \quad (3.2)$$

where C_{ij}^{-1} is the inverse covariance matrix. We assume that the covariance matrix is diagonal except of the WiggleZ subset of the data (three data points) where the covariance matrix has been published as

$$C_{ij}^{\text{WiggleZ}} = 10^{-3} \begin{pmatrix} 6.400 & 2.570 & 0.000 \\ 2.570 & 3.969 & 2.540 \\ 0.000 & 2.540 & 5.184 \end{pmatrix} \quad (3.3)$$

Notice that the C_{ij} nondiagonal element of the WiggleZ covariance matrix is well approximated as $C_{ij} \simeq 0.5\sqrt{C_{ii}C_{jj}}$. We use this approximation in what follows for the construction of Monte Carlo correlations among the $f\sigma_8$ data points in order to estimate the effects of the ignored correlations among the other datapoints. Thus the total covariance matrix takes the form

$$C_{ij}^{\text{growth, total}} = \begin{pmatrix} \sigma_1^2 & 0 & 0 & \dots \\ 0 & C_{ij}^{\text{WiggleZ}} & 0 & \dots \\ 0 & 0 & \dots & \sigma_N^2 \end{pmatrix} \quad (3.4)$$

where $N = 63$ corresponds to the number of data points of Table II. Clearly, this covariance matrix is an oversimplification as it ignores the existing correlations among various data points. Thus, in what follows we consider random variations with reasonable values of nondiagonal elements and identify the effects of these variations on the best fit parameter values and on the tension between these best fit values and Planck15/ Λ CDM.

Previous studies have indicated a wide range of tension levels between Planck15/ Λ CDM and the growth data depending mainly on the $f\sigma_8$ subsample they consider from the data set of Table II. For example Ref. [60] finds minimal to no tension with Planck15/ Λ CDM while Refs. [27,31] find about 3σ tension with Planck15/ Λ CDM. Thus a first question we want to address is: ‘‘What is the tension level for the full $f\sigma_8$ sample and what are the subsamples that maximize or minimize this tension?’’

In Fig. 4 (left panel) we show the $\Omega_{0m} - \sigma_8$ likelihood contours obtained from the full data set of Table II ignoring correlations but including fiducial model corrections. The Planck15/ Λ CDM contours are also shown. The tension between the best fit $\Omega_{0m} - \sigma_8$ and the Planck15/ Λ CDM values is at the 5σ level. The Planck15/ Λ CDM parameter values corresponds to higher values of both Ω_{0m} and σ_8 indicating stronger clustering than the indication of the actual data. This is also evident in Fig. 1 where the $f\sigma_8$ curve corresponding to Planck15/ Λ CDM is higher than the majority of the data points. The curve is lower and in better agreement with the full data set for the WMAP7/ Λ CDM parameter values that correspond to lower Ω_{0m} and σ_8 . This weaker clustering, compared with Planck15/ Λ CDM preferred by the growth data could be achieved in three ways: by decreasing the value of Ω_{0m} , by decreasing σ_8 or by decreasing G_{eff} at low redshifts [27].

The self consistency of the growth data set of Table II may be tested in several ways. One interesting consistency test is the comparison of the tension level with Planck15/ Λ CDM of the early published with the more recently published data. Thus in Figs. 4 (middle panel) and 4(right panel) we show the $\Omega_{0m} - \sigma_8$ likelihood contours

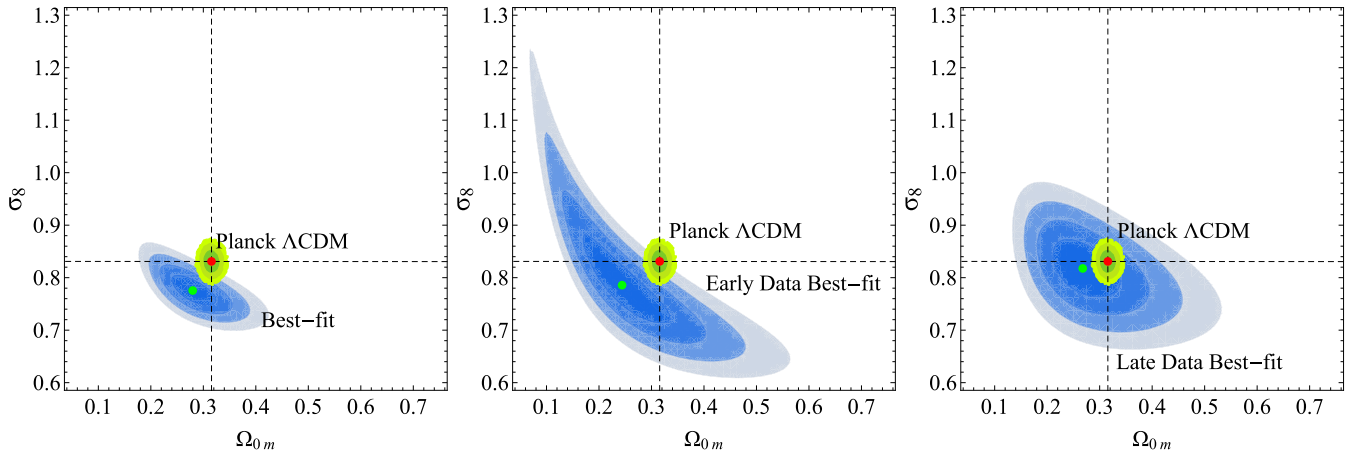


FIG. 4. The $1\sigma - 4\sigma$ confidence contours in the $(\Omega_{0m} - \sigma_8)$ parametric space. The blue contours correspond to the best fit of the 63 compilation data (left panel), the 20 early data (middle panel) and the 20 late data (right panel). The light green contours to the Planck15/ Λ CDM, while the red and green dots correspond to the Planck15/ Λ CDM best-fit cosmology and the best fit from the growth data respectively.

obtained using the 20 earliest published data (top 20 points in Table II where the points are ordered in accordance with time of publication) and the 20 most recently published data (bottom 20 points in Table II). As shown in Fig. 4 despite of the increase of the size of the contours due to the smaller number of data, the tension level remains at about 4σ when the early data are considered.

In contrast, when the late data are considered (see right panel in Fig. 4) the tension level decreases dramatically and the σ -distance between the best fit $\Omega_{0m} - \sigma_8$ parameters and the corresponding Planck15/ Λ CDM parameter values drops below 1σ . This dramatic decrease could be due to the following:

- (i) The fiducial models considered in early data points that were different from the Planck15/ Λ CDM fiducial model assumed in more recent studies. In order to estimate the effects of the assumed fiducial model

we reconstruct the contours of Fig. 4 without implementing the fiducial model correction described by Eq. (1.7). The new contours are shown in Fig. 5 for the full data set (left panel), for the 20 early data (middle panel) and for the 20 more recent data (right panel). The qualitative feature of the reduced tension for late data remains practically unaffected. Thus, the choice of the fiducial cosmology is not important in identifying the level of tension with Planck15/ Λ CDM.

This is also seen by plotting the correction factor $q(z, \Omega_{0m}^{\text{Planck15}}, \Omega_{0m})$ as a function of the redshift shown in Fig. 6 for various values of Ω_{0m} . The cosmological parameters of WMAP7/ Λ CDM are chosen as they represent well the fiducial models used for the 20 early $f\sigma_8$ data. Clearly, the difference of the correction factor from unity remains less than

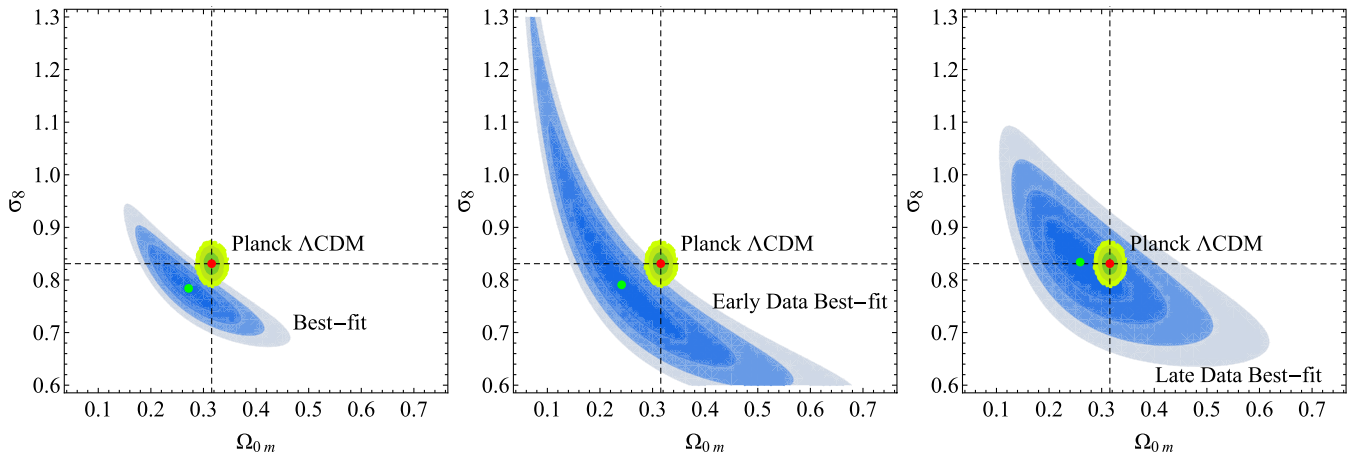


FIG. 5. Same as Fig. 4 but with no fiducial cosmology correction. The tension level in all three panels remains approximately the same.

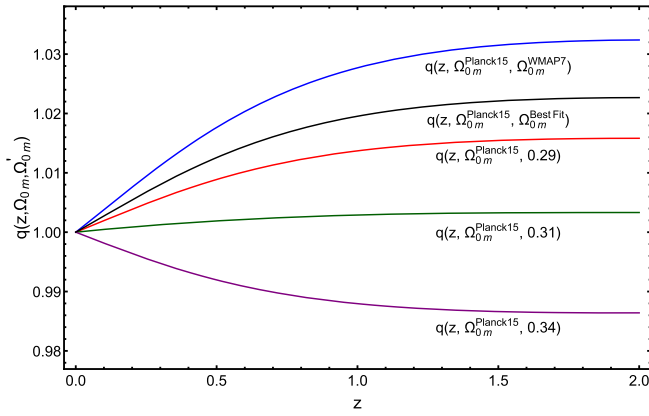


FIG. 6. The correction factor $q(z, \Omega_{0m}^{\text{Planck15}}, \Omega'_{0m})$ as a function of the redshift z .

3% for redshifts less than 1. This is much less than the typical level of error bars and explains the reduced role of the fiducial model in determining the tension level of the growth data with the Planck15/ Λ CDM parameter values.

- (ii) The covariance matrix which has been assumed to leave most of the data points uncorrelated. The effects of possible correlations among data points can be estimated by introducing a number of randomly selected nondiagonal elements in the covariance matrix while keeping it symmetric. In this approach we introduce positive correlations in 12 randomly selected pairs of data points (about 20% of the data). The positions of the nondiagonal elements are chosen randomly and the magnitude of the randomly selected covariance matrix element C_{ij} is set to

$$C_{ij} = 0.5\sigma_i\sigma_j \quad (3.5)$$

where $\sigma_i\sigma_j$ are the published 1σ errors of the data points i, j . The coefficient 0.5 is chosen in analogy with the magnitude of the nondiagonal elements of

the WiggleZ survey covariance matrix. The $\Omega_{0m} - \sigma_8$ likelihood contours corresponding to Fig. 4 with the use of a nontrivial covariance matrix constructed as described above, is shown in Fig. 7. The qualitative features of Figs. 7 and 4 remain similar for the full data set as well as the early data where there is 5σ tension with the Planck15/ Λ CDM parameter values while this tension disappears for the 20 most recently published data points. Thus the introduction of a nontrivial covariance matrix does not change the qualitative conclusions of our analysis which indicate a significant evolution (decrease) of the level of the tension with the time of publication of the $f\sigma_8$ data.

- (iii) Increased redshifts of more recent data points that probe redshift regions where different Λ CDM models make similar predictions as shown in Fig. 8 (bottom panel). This degeneracy is due to matter domination that appears in all viable models at early times. Due to the probe of higher redshifts the more recent data points also have larger error bars a fact that also make them less powerful in distinguishing among different models. The fact of increased redshifts and error bars for recent data points is demonstrated in what follows.
- (iv) Improved methods and reduced systematics may have lead to stronger evidence in favor of the concordance Planck15/ Λ CDM cosmological model.

To summarize, the sigma differences for all the cases of contours can be seen in the following Table III.

The trend for reduced tension of the growth data with Planck15/ Λ CDM may be seen more clearly by plotting the residuals of the data points of Fig. 1 with respect to the Planck15/ Λ CDM $f\sigma_8$ prediction. These residuals are defined as

$$\delta f\sigma_8(z_i) \equiv \frac{f\sigma_8(z_i)^{\text{data}} - f\sigma_8(z_i)^{\text{Planck15}}}{\sigma_i} \quad (3.6)$$

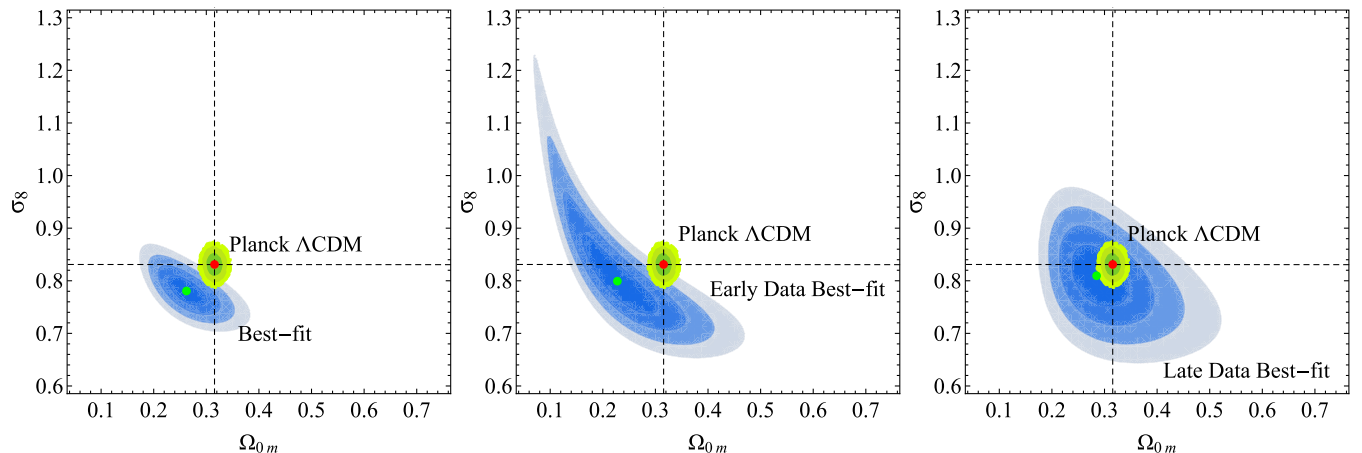


FIG. 7. Same as Fig. 4 but with a random covariance among 25% of the data points (assumed to be correlated in pairs). The tension level in all three panels remains approximately the same.

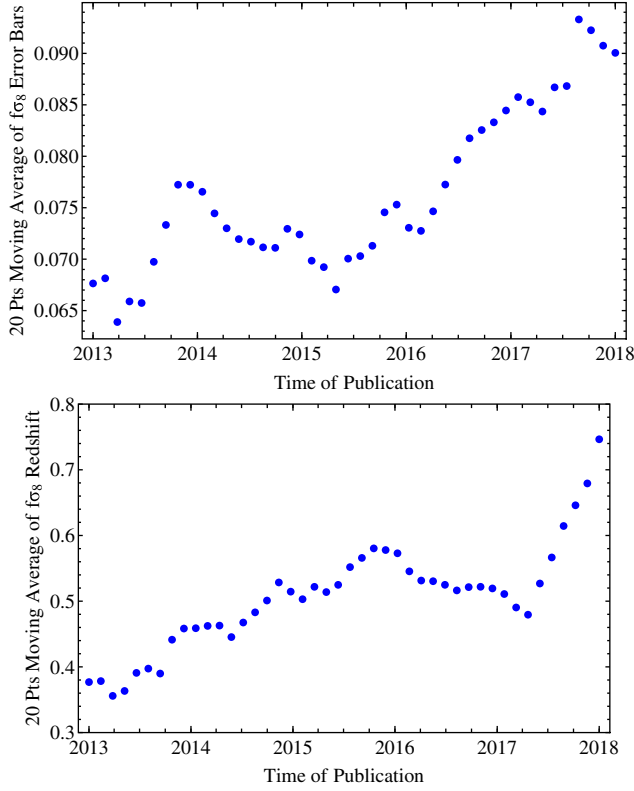


FIG. 8. Top panel: The 20 point moving average of $f\sigma_8$ error bars dependence on time of publication. Bottom panel: The 20 point moving average of $f\sigma_8$ redshifts dependence on time of publication.

In Fig. 9 we show these residual data points (with Planck15/ Λ CDM fiducial model corrections) ordered with respect to time of publication (top panel) and the corresponding N point moving average (bottom panel) setting $N = 20$. The moving average can be defined as

$$\overline{f\sigma_{8j}} \equiv \sum_{i=j-N}^j \frac{\delta f\sigma_8(z_i)}{N} \quad (3.7)$$

Clearly the consistency of the growth data with Planck15/ Λ CDM improves steadily with time of publication. The corresponding moving averages of the error bars and published data redshifts are shown in Fig. 8 indicating that both the moving average redshift and error bar increase with time of publication (top panel).

The increase of the average data redshift is to be expected due to the improvement of sensitivity of surveys.

TABLE III. Sigma differences of the best fit contours from the Planck15/ Λ CDM for Fig. 4, Fig. 5 and Fig. 7.

	Full dataset	Early data	Late data
Fig. 4 contours	4.97σ	3.89σ	0.94σ
Fig. 5 contours	5.44σ	4.36σ	0.97σ
Fig. 7 contours	4.76σ	4.77σ	0.37σ

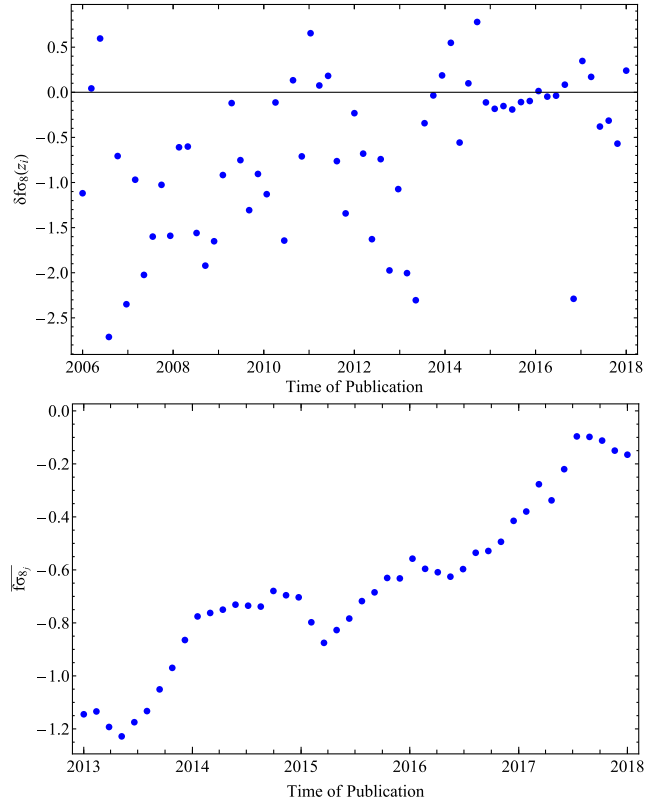


FIG. 9. Top panel: The residual of the datapoints with Planck15/ Λ CDM fiducial model correction based on Eq. (3.6). Bottom panel: The 20 points moving average defined by Eq. (3.7) with time of publication.

However, the increased error bars is an unexpected feature and deserves further investigation in view also of the fact that previous studies [28] have indicated that the $f\sigma_8$ error bars may be overestimated.

We thus address the following question: “Are the $f\sigma_8$ error bars of Table II consistent with the spread of the $f\sigma_8$ points?” In order to address this question we compare the variance of the real data $f\sigma_8$ residuals from their best fit Λ CDM with the variance of 100 Monte Carlo realizations of the corresponding residual data. In each Monte Carlo realization of the 63 residual data points, each data point is generated randomly from a Gaussian distribution with zero mean and standard deviation equal to the error bar of the real data point. The Monte Carlo variances are shown in Fig. 10 (100 red dots) along with the variance of the real data residuals (dotted line). The variance of the 100 Monte Carlo residual data sets is $\sigma_{MC}^2 = 0.0079 \pm 0.0015$ while the variance of the real data residuals is $\sigma_{RealData}^2 = 0.0030 \pm 0.055$.

This reduced variance of the real data could be due to either overestimation of the errors of the $f\sigma_8$ data of Table II or due to correlations/double counting in these data. In order to estimate the effects of correlations we introduce artificial double counting in the Monte Carlo data by enforcing 25% of the data points to have an identical

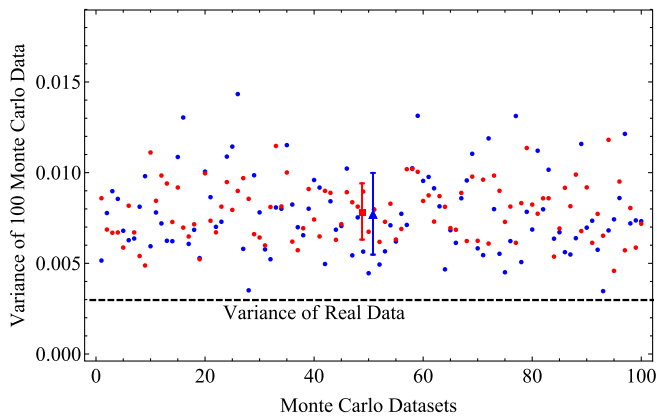


FIG. 10. The variances of 100 Monte Carlo data sets. Each red circular point provides the variance of a Monte Carlo residual data set with uncorrelated data, while each blue point provides the variance of a residual dataset with 25% double-counted data points (12 identical pairs of data points). The red square point describes the mean value of the uncorrelated data variances with the standard deviation whereas the blue triangular point is the mean value of the correlated data variances with one standard deviation.

corresponding data point is the Monte Carlo $f\sigma_8$ data set. The corresponding results after introducing artificial double counting in 25% of the Monte Carlo data can also be seen in Fig. 10 (blue points). In this case the variance of the Monte Carlo data becomes $\sigma_{MC}^2 = 0.0077 \pm 0.0023$ which is still significantly larger than the variance of the real data. Thus a moderate level of double-counting is not enough to explain the reduced spread of the real data. This implies that either the error bars of the $f\sigma_8$ data are indeed overestimated or that there are systematic effects that prevent the data from having the anticipated spread from the error bars.

B. Implications for modified gravity

The trend for reduced tension of the growth data with Planck15/ Λ CDM with time of publication implies also a trend for reduced indications for evolution of the effective Newton's constant G_{eff} . This trend is well parametrized by the parameter g_a of Eq. (2.13).

Assuming a Planck15/ Λ CDM background we fit the theoretically predicted $f\sigma_8(z, \Omega_{0m}^{\text{Planck15}}, \sigma_8^{\text{Planck15}}, g_a)$ obtained from Eqs. (2.2) and (2.14) to the full data set of Table II as well as to early and recent subsets in order to identify the evolution of the hints for modified gravity implied by the growth data. In Fig. 11 we show the 1σ range implied for g_a from the full $f\sigma_8$ data set, and for 20 point $f\sigma_8$ subsamples starting from the earliest subsample and ending with the most recent subsample.

The 1σ range for g_a using the full data set of Table II is $g_a = -0.91 \pm 0.17$ (red point). The 20 point subsample best fits start from $g_a = -1.28_{-0.26}^{+0.28}$ (earliest subsample) which is inconsistent with GR ($g_a = 0$) at about 4.5σ level

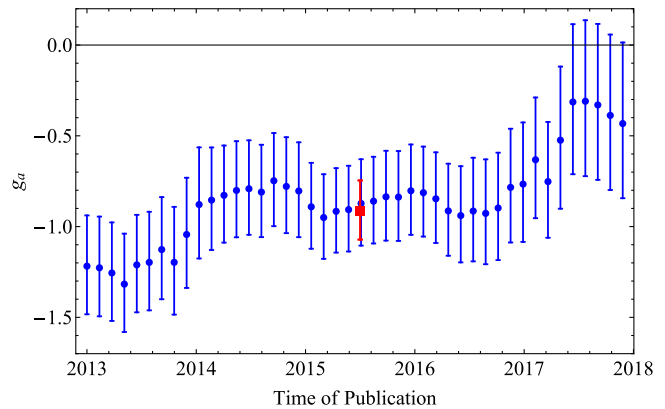


FIG. 11. The 1σ range implied for g_a from the full $f\sigma_8$ data set. Every blue point corresponds to the best fit g_a obtained from a 20 point $f\sigma_8$ subsample starting from the earliest subsample (on the left) to the latest (on the right). The red square point describes the best fit g_a obtained from the full data set along with the error bar.

and ends with the subsample of the 20 most recent data points which imply $g_a = -0.43_{-0.41}^{+0.46}$ which is less than 1σ away from the GR prediction $g_a = 0$.

IV. CONCLUSION-DISCUSSION

We have constructed a large $f\sigma_8$ growth data set which includes the vast majority (if not all) of the $f\sigma_8$ RSD data published to date by several redshift surveys. The data set consists of 63 distinct data points published by different surveys and/or at different times and to our knowledge is the largest $f\sigma_8$ compilations that has appeared in the literature so far. Even though this data set is plagued by correlations among data points and possible double counting it is still useful in identifying general trends of the data as well as the sensitivity of the best fit parameters to the fiducial model corrections and to correlations among the data points. Taking various subsamples of the full dataset we have demonstrated that the consistency of the published $f\sigma_8$ data with Planck15/ Λ CDM has improved significantly for the data published during the last 2–3 years. In fact for these data there is currently no tension with the Planck15/ Λ CDM in contrast with earlier data published before 2016 which are at about $3 - 5\sigma$ tension with Planck15/ Λ CDM. A partial cause for this reduced tension is the fact that more recent data tend to probe higher redshifts (with higher error bars) where there is degeneracy among different models due to matter domination. Thus probing redshifts less than one may be a more effective way for distinguishing among different cosmological models.

In addition we have demonstrated that a parametrization of the form of Eq. (2.15) provides an excellent fit to the product $f\sigma_8(z)$ obtained from the numerical solution of the Eq. (2.2) with Eq. (2.14) in both GR and in modified gravity theories.

TABLE IV. Sigma distances of the best fit parameter values of other growth sensitive data sets from the RSD data $\sigma_8 - \Omega_{0m}$ best fits.

Dataset	Full RSD dataset	Early RSD data	Late RSD data
KiDs data [22] ($\Omega_{0m} = 0.295^{+0.052}_{-0.087}$, $\sigma_8 = 0.747^{+0.093}_{-0.125}$)	1.17σ	0.42σ	1.50σ
Planck clusters data [121] ($\Omega_{0m} = 0.33 \pm 0.03$, $\sigma_8 = 0.76 \pm 0.03$)	1.21σ	1.52σ	1.23σ

Alternative data sets that directly probe the linear growth rate of density perturbations include weak lensing data (eg. KiDS [22,117] or the DES data [25,118–120]) and the Planck Sunyaev-Zeldovich (SZ) cluster counts [121]. Even though the preferred values of $\sigma_8 - \Omega_{0m}$ as obtained from the KiDS weak lensing data and from the Planck SZ cluster counts are in tension with the Planck analysis of primary fluctuations (Planck15/ Λ CDM) they are significantly more consistent with the RSD growth data. This fact is demonstrated in Table IV where we show the σ -distance of the KiDS and Planck cluster $\sigma_8 - \Omega_{0m}$ best fits from the RSD data $\sigma_8 - \Omega_{0m}$ best fit.

This Table indicates that the three sets of data that are probing directly the growth rate of cosmological fluctuations (weak lensing, RSD and Planck clusters) are consistent with each other but they are in some tension with the Planck analysis of primary fluctuations which is not as sensitive to the late redshift growth rate of perturbations. This effect could be viewed either as a hint of systematics in the data that probe directly the growth rate of density perturbations or as an early hint of new physics (perhaps of gravitational origin). The detailed investigation of this effect using both early and late weak lensing and cluster number counts data is an interesting extension of this analysis.

Other interesting extensions of the present work include the search for possible tensions between early and more recently published data in different data sets including geometric probes (SnIa and BAO) as well as dynamical growth probes such as weak lensing data. For example as mentioned above, the KiDs data have indicated significant tension with Planck15/ Λ CDM while this tension is not as strongly supported by other weak lensing data such as the DES data [25,118–120].

Finally, our analysis indicates all the $f\sigma_8$ subsamples indicate that G_{eff} has higher probability to be decreasing with redshift at low z than to be constant as indicated by GR. Thus it would be interesting to identify those modified gravity models that are consistent with this indication. This study is currently in progress.

Numerical analysis files: The numerical files for the reproduction of the figures can be found at <http://leandros.physics.uoi.gr/growth-tomography/>.

ACKNOWLEDGMENTS

We thank Savvas Nesseris for useful discussions.

APPENDIX: FIDUCIAL COSMOLOGY CORRECTION

The proper way to homogenize the data set with respect to different fiducial cosmologies would be to recalculate all the $f\sigma_8$ data points using the same fiducial cosmology in the construction of the correlation function. This approach is not practical as it would require a recalculation of $f\sigma_8(\Omega_{0m}, \sigma_8)$ for all parameter values (Ω_{0m}, σ_8) for which a value of χ^2 is to be calculated. An alternative approximate approach is the use of correction factors like the one of Eq. (1.7) which are obtained in the context of specific approximations. Such approaches include the following

- (i) The fiducial correction in Ref. [28], used in our analysis through Eq. (1.7). This correction factor tends to slightly increase the value of the $f\sigma_8$ data points when transforming from a WMAP7/ Λ CDM fiducial model to a Planck15/ Λ CDM model as shown in Fig. 1 of Ref. [28].
- (ii) The fiducial correction described in Ref. [56] where the transformation of $f\sigma_8$ from WMAP best fit cosmology [87] to the Planck best fit cosmology [122] is considered. Setting the WMAP7/ Λ CDM as the fiducial model and Planck15/ Λ CDM as the true cosmology, the relations between the corresponding three dimensional correlation functions taking into account the AP effect is

$$\xi_{\text{Planck}}(d\ell_{\parallel}, d\ell_{\perp}) = \xi_{\text{fid}}(f_{\parallel}d\ell_{\parallel}, f_{\perp}d\ell_{\perp}) \quad (\text{A1})$$

where $f_{\parallel} = H_{\text{fid}}/H_{\text{planck}}$, $f_{\perp} = D_A^{\text{planck}}/D_A^{\text{fid}}$. The corresponding relation between the $f\sigma_8$ under specific approximations (e.g., the bias is assumed proportional to σ_8) may be shown [56] to be

$$f\sigma_{8\text{Planck}} = f\sigma_{8\text{fid}} C \left(\frac{f_{\parallel}}{f_{\perp}^2} \right)^{(3/2)} \left(\frac{\sigma_8^{\text{planck}}}{\sigma_8^{\text{fid}}} \right)^2 \quad (\text{A2})$$

where $C = \int_{k_1}^{k_2} dk \sqrt{\frac{P_m^{\text{fid}}}{P_m^{\text{planck}}}} = \int_{k_1}^{k_2} dk \sqrt{\frac{P_m'}{P_m}}$. Substituting the definitions of f_{\parallel} and f_{\perp} , Eq. (1.7) takes the following form

$$q(z, \Omega_{0m}, \Omega'_{0m}) = C \left(\frac{H'(z)D'_A(z)^2}{H(z)D_A(z)^2} \right)^{3/2} \cdot \left(\frac{\sigma_8}{\sigma'_8} \right)^2 \quad (\text{A3})$$

Using Eq. (A3) for fiducial model correction in our analysis (setting $C = 1$) does not change the trend of reduced tension with Planck15/ Λ CDM for the more recent $f\sigma_8$ data. However it does reduce significantly

TABLE V. Sigma differences of the growth data best fit parameter values from the Planck15/ Λ CDM under the fiducial correction of Ref. [56].

	Full dataset	Early data	Late data
Correction factor (A3)	2.15σ	1.49σ	0.86σ
No correction	5.44σ	4.36σ	0.97σ
(A3) with random covariance	2.27σ	1.15σ	0.67σ

the overall tension of Planck15/ Λ CDM with the early data. The new tension levels in the context of the correction factor (A3) are shown in Table V

- (iii) An alternative fiducial correction factor [55] is written as

$$f\sigma'_8 = \left(\beta + \frac{n}{2} \left(1 - \frac{H'D'_A}{HD_A} \right) \right) b\sigma_8 \equiv f\sigma_8 + f\sigma_8^{\text{corr}} \quad (\text{A4})$$

where b is the bias, n is the logarithmic derivative of the power spectrum ($n = \frac{d \ln P}{d \ln k}$).

The practical implementation of correction factors (A3) and (A4) is not as straightforward as the implementation of Eq. (1.7) as the former require information about the power spectrum.

- [1] W. J. Percival, S. Cole, D. J. Eisenstein, R. C. Nichol, J. A. Peacock, A. C. Pope, and A. S. Szalay, Measuring the baryon acoustic oscillation scale using the SDSS and 2dFGRS, *Mon. Not. R. Astron. Soc.* **381**, 1053 (2007).
- [2] S. Alam *et al.* (BOSS), The clustering of galaxies in the completed SDSS-III Baryon Oscillation Spectroscopic Survey: cosmological analysis of the DR12 galaxy sample, *Mon. Not. R. Astron. Soc.* **470**, 2617 (2017).
- [3] M. Kowalski *et al.* (Supernova Cosmology Project), Improved cosmological constraints from new, old and combined supernova datasets, *Astrophys. J.* **686**, 749 (2008).
- [4] A. G. Riess *et al.*, New Hubble space telescope discoveries of type Ia supernovae at $z \geq 1$: Narrowing constraints on the early behavior of dark energy, *Astrophys. J.* **659**, 98 (2007).
- [5] A. H. Jaffe *et al.* (Boomerang), Cosmology from MAXIMA-1, BOOMERANG and COBE / DMR CMB Observations, *Phys. Rev. Lett.* **86**, 3475 (2001).
- [6] M. Hicken, W. Michael Wood-Vasey, S. Blondin, P. Challis, S. Jha, P. L. Kelly, A. Rest, and R. P. Kirshner, Improved dark energy constraints from 100 new CfA supernova type Ia light curves, *Astrophys. J.* **700**, 1097 (2009).
- [7] J. L. Sievers *et al.*, Cosmological parameters from cosmic background imager observations and comparisons with BOOMERANG, DASI, and MAXIMA, *Astrophys. J.* **591**, 599 (2003).
- [8] L. Izzo, M. Muccino, E. Zaninoni, L. Amati, and M. Della Valle, New measurements of Ω_m from gamma-ray bursts, *Astron. Astrophys.* **582**, A115 (2015).
- [9] M. Betoule *et al.* (SDSS), Improved cosmological constraints from a joint analysis of the SDSS-II and SNLS supernova samples, *Astron. Astrophys.* **568**, A22 (2014).
- [10] G. Efstathiou and P. Lemos, Statistical inconsistencies in the KiDS-450 dataset, [arXiv:1707.00483](https://arxiv.org/abs/1707.00483).
- [11] S. M. Carroll, The cosmological constant, *Living Rev. Relativity* **4**, 1 (2001).
- [12] P. A. R. Ade *et al.* (Planck), Planck 2015 results. XIII. Cosmological parameters, *Astron. Astrophys.* **594**, A13 (2016).
- [13] S. Perlmutter *et al.* (Supernova Cosmology Project), Measurements of Omega and Lambda from 42 high redshift supernovae, *Astrophys. J.* **517**, 565 (1999).
- [14] A. G. Riess *et al.* (Supernova Search Team), Observational evidence from supernovae for an accelerating universe and a cosmological constant, *Astron. J.* **116**, 1009 (1998).
- [15] N. Suzuki *et al.*, The Hubble space telescope cluster supernova survey: V. Improving the dark energy constraints above $z > 1$ and building an early-type-hosted supernova sample, *Astrophys. J.* **746**, 85 (2012).
- [16] P. Bull *et al.*, Beyond Λ CDM: Problems, solutions, and the road ahead, *Phys. Dark Universe* **12**, 56 (2016).
- [17] J. Solà, Cosmological constant vis-a-vis dynamical vacuum: Bold challenging the Λ CDM, *Int. J. Mod. Phys. A* **31**, 1630035 (2016).
- [18] W. Lin and M. Ishak, Cosmological discordances II: Hubble constant, Planck and large-scale-structure data sets, *Phys. Rev. D* **96**, 083532 (2017).
- [19] W. Lin and M. Ishak, Cosmological discordances: A new measure, marginalization effects, and application to geometry versus growth current data sets, *Phys. Rev. D* **96**, 023532 (2017).
- [20] V. Sahni, A. Shafieloo, and A. A. Starobinsky, Model independent evidence for dark energy evolution from baryon acoustic oscillations, *Astrophys. J.* **793**, L40 (2014).
- [21] H. Hildebrandt *et al.*, KiDS-450: Cosmological parameter constraints from tomographic weak gravitational lensing, *Mon. Not. R. Astron. Soc.* **465**, 1454 (2017).
- [22] S. Joudaki *et al.*, KiDS-450 + 2dFLenS: Cosmological parameter constraints from weak gravitational lensing tomography and overlapping redshift-space galaxy clustering, *Mon. Not. R. Astron. Soc.* **474**, 4894 (2018).
- [23] M. James Jee, J. Anthony Tyson, S. Hilbert, M. D. Schneider, S. Schmidt, and D. Wittman, Cosmic shear

- results from the deep lens survey—II: Full cosmological parameter constraints from tomography, *Astrophys. J.* **824**, 77 (2016).
- [24] T. Abbott *et al.* (DES), Cosmology from cosmic shear with Dark Energy Survey Science Verification data, *Phys. Rev. D* **94**, 022001 (2016).
- [25] M. A. Troxel *et al.* (DES), Dark energy survey year 1 results: Cosmological constraints from cosmic shear, [arXiv:1708.01538](https://arxiv.org/abs/1708.01538).
- [26] F. Köhlinger *et al.*, KiDS-450: The tomographic weak lensing power spectrum and constraints on cosmological parameters, *Mon. Not. R. Astron. Soc.* **471**, 4412 (2017).
- [27] S. Nesseris, G. Pantazis, and L. Perivolaropoulos, Tension and constraints on modified gravity parametrizations of $G_{\text{eff}}(z)$ from growth rate and Planck data, *Phys. Rev. D* **96**, 023542 (2017).
- [28] E. Macaulay, I. K. Wehus, and H. K. Eriksen, Lower Growth Rate from Recent Redshift Space Distortion Measurements than Expected from Planck, *Phys. Rev. Lett.* **111**, 161301 (2013).
- [29] S. Tsujikawa, Possibility of realizing weak gravity in redshift space distortion measurements, *Phys. Rev. D* **92**, 044029 (2015).
- [30] A. Johnson, C. Blake, J. Dossett, J. Koda, D. Parkinson, and S. Joudaki, Searching for modified gravity: Scale and redshift dependent constraints from galaxy peculiar velocities, *Mon. Not. R. Astron. Soc.* **458**, 2725 (2016).
- [31] S. Basilakos and S. Nesseris, Conjoined constraints on modified gravity from the expansion history and cosmic growth, *Phys. Rev. D* **96**, 063517 (2017).
- [32] S. Capozziello and M. De Laurentis, Extended theories of gravity, *Phys. Rep.* **509**, 167 (2011).
- [33] Y.-F. Cai, C. Li, E. N. Saridakis, and L. Xue, $f(T)$ gravity after GW170817 and GRB170817A, [arXiv:1801.05827](https://arxiv.org/abs/1801.05827).
- [34] J. Pérez-Romero and S. Nesseris, Cosmological constraints and comparison of viable $f(R)$ models, *Phys. Rev. D* **97**, 023525 (2018).
- [35] W. Hu and I. Sawicki, Models of $f(R)$ cosmic acceleration that evade solar-system tests, *Phys. Rev. D* **76**, 064004 (2007).
- [36] L. Boubekur, E. Giusarma, O. Mena, and H. Ramírez, Current status of modified gravity, *Phys. Rev. D* **90**, 103512(2014).
- [37] R. Gannouji, B. Moraes, and D. Polarski, The growth of matter perturbations in $f(R)$ models, *J. Cosmol. Astropart. Phys.* **02** (2009) 034.
- [38] S. Tsujikawa, Matter density perturbations and effective gravitational constant in modified gravity models of dark energy, *Phys. Rev. D* **76**, 023514 (2007).
- [39] E. Massaelli, M. Motaharfari, and H. R. Sepangi, General scalar-tensor cosmology: analytical solutions via noether symmetry, *Eur. Phys. J. C* **77**, 124 (2017).
- [40] A. De Felice, T. Kobayashi, and S. Tsujikawa, Effective gravitational couplings for cosmological perturbations in the most general scalar-tensor theories with second-order field equations, *Phys. Lett. B* **706**, 123 (2011).
- [41] V. Sahni and Y. Shtanov, Brane world models of dark energy, *J. Cosmol. Astropart. Phys.* **11** (2004) 014.
- [42] U. Alam, S. Bag, and V. Sahni, Constraining the cosmology of the phantom brane using distance measures, *Phys. Rev. D* **95**, 023524 (2017).
- [43] E. A. Novikov, Ultralight gravitons with tiny electric dipole moment are seeping from the vacuum, *Mod. Phys. Lett. A* **31**, 1650092 (2016).
- [44] E. A. Novikov, Quantum modification of general relativity, *Electron. J. Theor. Phys.* **13**, 79–90 (2016).
- [45] D. Larson *et al.*, Seven-year Wilkinson Microwave Anisotropy Probe (WMAP) observations: Power spectra and WMAP-derived parameters, *Astrophys. J. Suppl. Ser.* **192**, 16 (2011).
- [46] C. Blake *et al.*, The WiggleZ Dark Energy Survey: joint measurements of the expansion and growth history at $z1$, *Mon. Not. R. Astron. Soc.* **425**, 405 (2012).
- [47] D. Heath Jones *et al.*, The 6dF Galaxy Survey: Samples, observational techniques and the first data release, *Mon. Not. R. Astron. Soc.* **355**, 747 (2004).
- [48] S. Alam *et al.* (SDSS-III), The eleventh and twelfth data releases of the Sloan Digital Sky Survey: Final data from SDSS-III, *Astrophys. J. Suppl. Ser.* **219**, 12 (2015).
- [49] Y. Wang, G.-B. Zhao, C.-H. Chuang, M. Pellejero-Ibanez, C. Zhao, F.-S. Kitaura, and S. Rodriguez-Torres, The clustering of galaxies in the completed SDSS-III Baryon Oscillation Spectroscopic Survey: a tomographic analysis of structure growth and expansion rate from anisotropic galaxy clustering, [arXiv:1709.05173](https://arxiv.org/abs/1709.05173).
- [50] L. Guzzo *et al.*, The VIMOS Public Extragalactic Redshift Survey (VIPERS), *Astron. Astrophys.* **566**, A108 (2014).
- [51] N. Kaiser, Clustering in real space and in redshift space, *Mon. Not. R. Astron. Soc.* **227**, 1 (1987).
- [52] X.-D. Li, C. Park, C. G. Sabiu, H. Park, D. H. Weinberg, D. P. Schneider, J. Kim, and S. E. Hong, Cosmological constraints from the redshift dependence of the Alcock-Paczynski effect: application to the SDSS-III BOSS DR12 galaxies, *Astrophys. J.* **832**, 103 (2016).
- [53] N. Padmanabhan and M. J. White, Constraining anisotropic baryon oscillations, *Phys. Rev. D* **77**, 123540 (2008).
- [54] S. Saito, Lecture notes in cosmology (2016).
- [55] M. J. Wilson, Ph.D. thesis, Edinburgh U., 2016; Geometric and growth rate tests of General Relativity with recovered linear cosmological perturbations, [arXiv:1610.08362](https://arxiv.org/abs/1610.08362).
- [56] S. Alam, S. Ho, and A. Silvestri, Testing deviations from Λ CDM with growth rate measurements from six large-scale structure surveys at $z = 0.06-1$, *Mon. Not. R. Astron. Soc.* **456**, 3743 (2016).
- [57] C. Alcock and B. Paczynski, An evolution free test for non-zero cosmological constant, *Nature (London)* **281**, 358 (1979).
- [58] A. Gomez-Valent and J. Sola, Relaxing the σ_8 -tension through running vacuum in the Universe, *Europhys. Lett.* **120**, 39001 (2017).
- [59] A. Gómez-Valent and J. Solà, Density perturbations for running vacuum: A successful approach to structure formation and to the σ_8 -tension, [arXiv:1801.08501](https://arxiv.org/abs/1801.08501).
- [60] S. Basilakos and S. Nesseris, Testing Einstein’s gravity and dark energy with growth of matter perturbations: Indications for new physics?, *Phys. Rev. D* **94**, 123525 (2016).

- [61] S. Nesseris and D. Sapone, Novel null-test for the Λ cold dark matter model with growth-rate data, *Int. J. Mod. Phys. D* **24**, 1550045 (2015).
- [62] A. Mehrabi, S. Basilakos, M. Malekjani, and Z. Davari, Growth of matter perturbations in clustered holographic dark energy cosmologies, *Phys. Rev. D* **92**, 123513 (2015).
- [63] T. Baker, P. G. Ferreira, C. D. Leonard, and M. Motta, New gravitational scales in cosmological surveys, *Phys. Rev. D* **90**, 124030 (2014).
- [64] S. Nesseris and L. Perivolaropoulos, Testing Lambda CDM with the growth function $\delta(a)$: Current constraints, *Phys. Rev. D* **77**, 023504 (2008).
- [65] S. Basilakos, The growth index of matter perturbations using the clustering of dark energy, *Mon. Not. R. Astron. Soc.* **449**, 2151 (2015).
- [66] A. Pouri, S. Basilakos, and M. Plionis, Precision growth index using the clustering of cosmic structures and growth data, *J. Cosmol. Astropart. Phys.* **08** (2014) 042.
- [67] B. C. Paul and P. Thakur, Observational constraints on modified Chaplygin gas from cosmic growth, *J. Cosmol. Astropart. Phys.* **11** (2013) 052.
- [68] B. L'Huillier, A. Shafieloo, and H. Kim, Model-independent cosmological constraints from growth and expansion, [arXiv:1712.04865](https://arxiv.org/abs/1712.04865).
- [69] Y.-S. Song and W. J. Percival, Reconstructing the history of structure formation using redshift distortions, *J. Cosmol. Astropart. Phys.* **10** (2009) 004.
- [70] Max Tegmark *et al.* (SDSS), Cosmological constraints from the SDSS luminous red galaxies, *Phys. Rev. D* **74**, 123507 (2006).
- [71] M. Davis, A. Nusser, K. Masters, C. Springob, J. P. Huchra, and G. Lemson, Local gravity versus local velocity: Solutions for β and nonlinear bias, *Mon. Not. R. Astron. Soc.* **413**, 2906 (2011).
- [72] M. J. Hudson and S. J. Turnbull, The growth rate of cosmic structure from peculiar velocities at low and high redshifts, *Astrophys. J. Lett.* **751**, L30 (2012).
- [73] S. J. Turnbull, M. J. Hudson, H. A. Feldman, M. Hicken, R. P. Kirshner, and R. Watkins, Cosmic flows in the nearby universe from type Ia supernovae, *Mon. Not. R. Astron. Soc.* **420**, 447 (2012).
- [74] L. Samushia, W. J. Percival, and A. Raccanelli, Interpreting large-scale redshift-space distortion measurements, *Mon. Not. R. Astron. Soc.* **420**, 2102 (2012).
- [75] F. Beutler, C. Blake, M. Colless, D. Heath Jones, L. Staveley-Smith, G. B. Poole, L. Campbell, Q. Parker, W. Saunders, and F. Watson, The 6df galaxy survey: $z \approx 0$ measurements of the growth rate and σ_8 , *Mon. Not. R. Astron. Soc.* **423**, 3430 (2012).
- [76] R. Tojeiro *et al.*, The clustering of galaxies in the sdss-iii baryon oscillation spectroscopic survey: measuring structure growth using passive galaxies, *Mon. Not. R. Astron. Soc.* **424**, 2339 (2012).
- [77] S. de la Torre *et al.*, The VIMOS Public Extragalactic Redshift Survey (VIPERS). Galaxy clustering and redshift-space distortions at $z = 0.8$ in the first data release, *Astron. Astrophys.* **557**, A54 (2013).
- [78] C.-H. Chuang and Y. Wang, Modelling the anisotropic two-point galaxy correlation function on small scales and single-probe measurements of $h(z)$, $da(z)$ and $f(z)\sigma_8(z)$ from the sloan digital sky survey dr7 luminous red galaxies, *Mon. Not. R. Astron. Soc.* **435**, 255 (2013).
- [79] E. Komatsu *et al.* (WMAP), Seven-Year Wilkinson Microwave Anisotropy Probe (WMAP) observations: Cosmological interpretation, *Astrophys. J. Suppl. Ser.* **192**, 18 (2011).
- [80] C. Blake *et al.*, Galaxy And Mass Assembly (GAMA): Improved cosmic growth measurements using multiple tracers of large-scale structure, *Mon. Not. R. Astron. Soc.* **436**, 3089 (2013).
- [81] A. G. Sanchez *et al.*, The clustering of galaxies in the SDSS-III Baryon Oscillation Spectroscopic Survey: Cosmological implications of the full shape of the clustering wedges in the data release 10 and 11 galaxy samples, *Mon. Not. R. Astron. Soc.* **440**, 2692 (2014).
- [82] Lauren Anderson *et al.* (BOSS), The clustering of galaxies in the SDSS-III Baryon Oscillation Spectroscopic Survey: baryon acoustic oscillations in the Data Releases 10 and 11 Galaxy samples, *Mon. Not. R. Astron. Soc.* **441**, 24 (2014).
- [83] C. Howlett, A. Ross, L. Samushia, Will Percival, and M. Manera, The clustering of the SDSS main galaxy sample—II. Mock galaxy catalogues and a measurement of the growth of structure from redshift space distortions at $z = 0.15$, *Mon. Not. R. Astron. Soc.* **449**, 848 (2015).
- [84] M. Feix, A. Nusser, and E. Branchini, Growth Rate of Cosmological Perturbations at $z \approx 0.1$ from a New Observational Test, *Phys. Rev. Lett.* **115**, 011301 (2015).
- [85] Max Tegmark *et al.* (SDSS), The 3-D power spectrum of galaxies from the SDSS, *Astrophys. J.* **606**, 702 (2004).
- [86] T. Okumura *et al.*, The Subaru FMOS galaxy redshift survey (FastSound). IV. New constraint on gravity theory from redshift space distortions at $z \sim 1.4$, *Publ. Astron. Soc. Jpn.* **68**, 38 (2016).
- [87] G. Hinshaw *et al.* (WMAP), Nine-Year Wilkinson Microwave Anisotropy Probe (WMAP) observations: Cosmological parameter results, *Astrophys. J. Suppl. Ser.* **208**, 19 (2013).
- [88] C.-H. Chuang *et al.*, The clustering of galaxies in the SDSS-III Baryon Oscillation Spectroscopic Survey: single-probe measurements from CMASS anisotropic galaxy clustering, *Mon. Not. R. Astron. Soc.* **461**, 3781 (2016).
- [89] F. Beutler *et al.* (BOSS), The clustering of galaxies in the completed SDSS-III Baryon Oscillation Spectroscopic Survey: Anisotropic galaxy clustering in Fourier-space, *Mon. Not. R. Astron. Soc.* **466**, 2242 (2017).
- [90] H. Gil-Marín, W. J. Percival, Licia Verde, J. R. Brownstein, C.-H. Chuang, F.-S. Kitaura, S. A. Rodríguez-Torres, and M. D. Olmstead, The clustering of galaxies in the SDSS-III Baryon Oscillation Spectroscopic Survey: RSD measurement from the power spectrum and bispectrum of the DR12 BOSS galaxies, *Mon. Not. R. Astron. Soc.* **465**, 1757 (2017).
- [91] A. J. Hawken *et al.*, The VIMOS Public Extragalactic Redshift Survey: Measuring the growth rate of structure around cosmic voids, *Astron. Astrophys.* **607**, A54 (2017).
- [92] D. Huterer, D. Shafer, D. Scolnic, and F. Schmidt, Testing Λ CDM at the lowest redshifts with SN Ia and galaxy velocities, *J. Cosmol. Astropart. Phys.* **05** (2017) 015.

- [93] S. de la Torre *et al.*, The VIMOS Public Extragalactic Redshift Survey (VIPERS). Gravity test from the combination of redshift-space distortions and galaxy-galaxy lensing at $0.5 < z < 1.2$, *Astron. Astrophys.* **608**, A44 (2017).
- [94] A. Pezzotta *et al.*, The VIMOS Public Extragalactic Redshift Survey (VIPERS): The growth of structure at $0.5 < z < 1.2$ from redshift-space distortions in the clustering of the PDR-2 final sample, *Astron. Astrophys.* **604**, A33 (2017).
- [95] M. Feix, E. Branchini, and A. Nusser, Speed from light: Growth rate and bulk flow at $z \approx 0.1$ from improved SDSS DR13 photometry, *Mon. Not. R. Astron. Soc.* **468**, 1420 (2017).
- [96] C. Howlett, L. Staveley-Smith, P. J. Elahi, T. Hong, T. H. Jarrett, D. Heath Jones, B. S. Koribalski, L. M. Macri, K. L. Masters, and C. M. Springob, 2MTF VI. Measuring the velocity power spectrum, *Mon. Not. R. Astron. Soc.* **471**, 3135 (2017).
- [97] F. G. Mohammad *et al.*, The VIMOS Public Extragalactic Redshift Survey (VIPERS): An unbiased estimate of the growth rate of structure at $\langle z \rangle = 0.85$ using the clustering of luminous blue galaxies, *Astron. Astrophys.* **610**, A59 (2018).
- [98] F. Shi *et al.*, Mapping the Real Space Distributions of Galaxies in SDSS DR7: II. Measuring the growth rate, linear mass variance and biases of galaxies at redshift 0.1, [arXiv:1712.04163](https://arxiv.org/abs/1712.04163).
- [99] H. Gil-Marín *et al.*, The clustering of the SDSS-IV extended Baryon Oscillation Spectroscopic Survey DR14 quasar sample: structure growth rate measurement from the anisotropic quasar power spectrum in the redshift range $0.8 < z < 2.2$, [arXiv:1801.02689](https://arxiv.org/abs/1801.02689).
- [100] J. Hou *et al.*, The clustering of the SDSS-IV extended Baryon Oscillation Spectroscopic Survey DR14 quasar sample: anisotropic clustering analysis in configuration-space, [arXiv:1801.02656](https://arxiv.org/abs/1801.02656).
- [101] G.-B. Zhao *et al.*, The clustering of the SDSS-IV extended Baryon Oscillation Spectroscopic Survey DR14 quasar sample: a tomographic measurement of cosmic structure growth and expansion rate based on optimal redshift weights, [arXiv:1801.03043](https://arxiv.org/abs/1801.03043).
- [102] L.-M. Wang and P. J. Steinhardt, Cluster abundance constraints on quintessence models, *Astrophys. J.* **508**, 483 (1998).
- [103] E. V. Linder, Cosmic growth history and expansion history, *Phys. Rev. D* **72**, 043529 (2005).
- [104] D. Polarski and R. Gannouji, On the growth of linear perturbations, *Phys. Lett. B* **660**, 439 (2008).
- [105] R. Gannouji and D. Polarski, The growth of matter perturbations in some scalar-tensor DE models, *J. Cosmol. Astropart. Phys.* **05** (2008) 018.
- [106] D. Polarski, A. A. Starobinsky, and H. Giacomini, When is the growth index constant?, *J. Cosmol. Astropart. Phys.* **12** (2016) 037.
- [107] S. Nesseris and D. Sapone, Accuracy of the growth index in the presence of dark energy perturbations, *Phys. Rev. D* **92**, 023013 (2015).
- [108] A. Lykkas and L. Perivolaropoulos, Scalar-tensor quintessence with a linear potential: Avoiding the big crunch cosmic doomsday, *Phys. Rev. D* **93**, 043513 (2016).
- [109] B. Boisseau, G. Esposito-Farese, D. Polarski, and A. A. Starobinsky, Reconstruction of a Scalar Tensor Theory of Gravity in an Accelerating Universe, *Phys. Rev. Lett.* **85**, 2236 (2000).
- [110] G. Esposito-Farese and D. Polarski, Scalar tensor gravity in an accelerating universe, *Phys. Rev. D* **63**, 063504 (2001).
- [111] L. Perivolaropoulos, Crossing the phantom divide barrier with scalar tensor theories, *J. Cosmol. Astropart. Phys.* **10** (2005) 001.
- [112] S. Nesseris and L. Perivolaropoulos, The limits of extended quintessence, *Phys. Rev. D* **75**, 023517 (2007).
- [113] C. J. Copi, A. N. Davis, and L. M. Krauss, A New Nucleosynthesis Constraint on the Variation of G, *Phys. Rev. Lett.* **92**, 171301 (2004).
- [114] W. J. Percival, Cosmological structure formation in a homogeneous dark energy background, *Astron. Astrophys.* **443**, 819 (2005).
- [115] A. B. Belloso, J. Garcia-Bellido, and D. Sapone, A parametrization of the growth index of matter perturbations in various Dark Energy models and observational prospects using a Euclid-like survey, *J. Cosmol. Astropart. Phys.* **10** (2011) 010.
- [116] V. Silveira and I. Waga, Decaying Lambda cosmologies and power spectrum, *Phys. Rev. D* **50**, 4890 (1994).
- [117] A. Amon *et al.*, KiDS + 2dFLenS + GAMA: Testing the cosmological model with the E_G statistic, [arXiv:1711.10999](https://arxiv.org/abs/1711.10999).
- [118] E. J. Baxter *et al.*, Dark Energy Survey year 1 results: Methodology and projections for joint analysis of galaxy clustering, galaxy lensing, and CMB lensing two-point functions, [arXiv:1802.05257](https://arxiv.org/abs/1802.05257).
- [119] N. Jeffrey *et al.* (DES), Improving weak lensing mass map reconstructions using Gaussian and sparsity priors: Application to DES SV, [arXiv:1801.08945](https://arxiv.org/abs/1801.08945).
- [120] T. M. C. Abbott *et al.* (DES), The Dark Energy Survey data release 1, [arXiv:1801.03181](https://arxiv.org/abs/1801.03181).
- [121] P. A. R. Ade *et al.* (Planck), Planck 2015 results. XXIV. Cosmology from Sunyaev-Zeldovich cluster counts, *Astron. Astrophys.* **594**, A24 (2016).
- [122] P. A. R. Ade *et al.* (Planck), Planck 2013 results. I. Overview of products and scientific results, *Astron. Astrophys.* **571**, A1 (2014).